ACS MATERIALS LETTERS

www.acsmaterialsletters.org

REVIEW

Far-From-Equilibrium Processing Opens Kinetic Paths for Engineering Novel Materials by Breaking Thermodynamic Limits

Yihong Yu, Zhengpeng Qin, Xuefeng Zhang, Yanan Chen, Gaowu Qin, and Song Li*

Cite This: *ACS Materials Lett.* 2025, 7, 319−332

Read Online

ACCESS | Metrics & More | Article Recommendations

ABSTRACT: Thermodynamic metastable nanomaterials display attractive properties due to their unique atom configuration and microstructure, distinct from their counterparts found in equilibrium phase diagrams. However, their fabrication remains a grand challenge because conventional methods are generally operated under near-equilibrium conditions. To break the thermodynamic limits for discovering novel materials, numerous fabrication methods by adopting extreme strategies have been developed, including ultrafast synthesis, Joule heating, carbon thermal shock, pulse heating, extreme temperature gradients, and rapid solidification. A common feature of these methods is that the target material is processed under a far-from-equilibrium (FFE) thermodynamic state, where a new kinetic route is created for the evolution of an unprecedented composition/structure. In this review, we provide a unifying view and guiding strategies for engineering FFE environments during materials synthesis, categorized within both temporal and spatial dimensions of the thermodynamic landscape. Furthermore, we highlight the potential of FFE materials, not only as platforms for deeper understanding nonequilibrium behaviors, but also as a framework for designing innovative materials for advanced technologies.

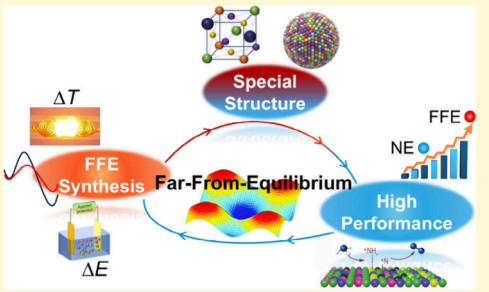

Novel and high-performance materials play a crucial role in advancing high-technologies and addressing sustainability challenges.[1,2] A primary scientific objective in materials research is to develop synthesis and treatment strategies that yield materials with exceptional properties for diverse applications by precise atomic manipulation.[3,4] In energy harvesting and conversion, for instance, nanoscale electrocatalysts efficiently convert renewable electricity into chemical energy, paving the way for a sustainable future.[5−7] Lightweight yet robust alloys engineered through advanced manufacturing techniques enable fuel-efficient transportation.[8−10] Due to the vast diversity of materials, numerous processing methods, including top-down and bottom-up, have been developed to create target materials with tunable composition, morphology, size, and microstructure.[11,12] Despite significant advancement, materials developed to date are dominated by thermodynamically stable phases and microstructures,[13] as most synthesis methods operate under near-equilibrium thermodynamic conditions. This thermodynamic constraint limits the discovery of promising materials that inherently exist far from equilibrium.[14] To overcome this constraint and broaden the scope of material exploration, it is essential to develop new synthesis methodologies with distinct thermodynamic and kinetics features.

Materials processing for synthesis purposes is the art of manipulating atoms. A multitude of individual subprocesses of atomic movement is involved, ultimately shaping the final structure of the final material through a balance of interconnected subprocesses.[15,16] For example, the solution synthesis of multicomponent alloy nanostructures for catalysis involves a series of distinct subprocesses: reduction of metal salt precursors, nucleation, alloying driven by interfacial energy minimization, and nanostructure growth.[17,18] Each step is influenced by thermodynamic factors such as temperature, constituent concentration, and surfactant presence, which together shape the final structure.[19−21] While high temperatures favor alloying and uniform distribution of multiple elements, they can be detrimental to achieving high specific

Received: September 23, 2024
Revised: November 25, 2024
Accepted: December 10, 2024
Published: December 20, 2024

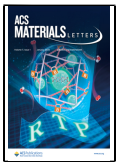

https://doi.org/10.1021/acsmaterialslett.4c01952
ACS Materials Lett. 2025, 7, 319−332

surface area due to coarsening.[22] Thus, synthesis is far more complex than mere mixing and heating; it is a symphony of atomic movements guided by thermodynamic principles and orchestrated by experimental conditions. Understanding and controlling these processes are essential for designing and fabricating materials with tailored properties for diverse applications.[23]

To fabricate materials with optimal microstructure, the interplayed subprocesses must be decoupled to ensure that only the desired processes proceed at a dominant rate. A significant challenge lies in simultaneously controlling thermodynamic and kinetic factors to selectively accelerate a specific subprocess while freezing the others.[24,25] Achieving this often requires extreme processing conditions, such as rapid heating, cooling, or the application of electric fields, to direct the material into configurations that traditional near-equilibrium methods cannot reach. Due to its potential to address the challenge, far-from-equilibrium (FFE) processing has attracted significant scientific attention recently. For instance, Hu et al. demonstrated that a heating pulse can resolve the conflict of alloying and particle growth.[14] By rapidly heating precursors to temperatures exceeding 1500 K within subseconds, they successfully produced high entropy nanoparticles in solid-solution state with uniform distribution,[26] and even the mixed metals are immiscible under thermodynamic equilibrium.[27] The core concept underlying FFE synthesis involves subjecting the system to extreme environments during fabrication, thereby allowing nonequilibrium microstructures to be kinetically trapped. Recent advances have introduced various FFE strategies, enabling the fabrication of materials with compositions and structures significantly different from those achievable at or near equilibrium. Consequently, FFE processing represents a paradigm shift in materials science, opening up new possibilities for creating structures and functionalities unattainable through conventional near-equilibrium methods.[23]

The core concept underlying FFE synthesis involves subjecting the system to extreme environments during fabrication, thereby allowing nonequilibrium microstructures to be kinetically trapped. Recent advances have introduced various FFE strategies, enabling the fabrication of materials with compositions and structures significantly different from those achievable at or near equilibrium. Consequently, FFE processing represents a paradigm shift in materials science, opening up new possibilities for creating structures and functionalities unattainable through conventional near-equilibrium methods.

This review provides a comprehensive examination of the fundamentals and applications of FFE strategies for materials processing, focusing on methods that manipulate the thermodynamic Gibbs free energy (ΔG). Particular emphasis is placed on the effects of varying the temperature (ΔT) and voltage (ΔE). We discuss the underlying principles, challenges, and opportunities associated with far-from-equilibrium materials, highlighting their distinctive properties that make them well-suited for a wide range of applications. Moreover, we present recent advancements in the preparation of both functional and structural materials using FFE techniques, illustrated with specific examples. We hope this review inspires fresh ideas for designing materials with broad applications and fosters further innovations in the field of materials science.

FUNDAMENTALS OF FAR-FROM-EQUILIBRIUM PROCESSING

Far-from-equilibrium (FFE) behaviors are pervasive in nature and material systems.[28] During material synthesis, whether through precursor-to-product conversion or phase transformations, the free energy is determined by key thermodynamic parameters such as the temperature, pressure, and applied potential (as illustrated in Figure 1). While

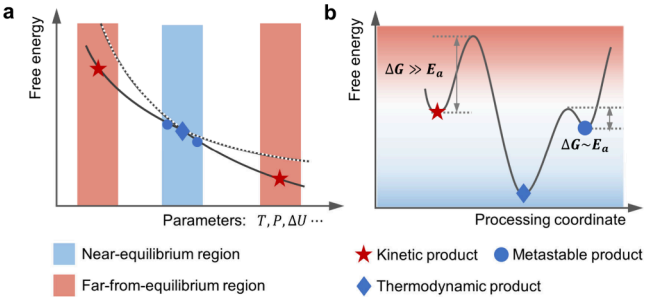

Figure 1. Potential energy landscape schematically illustrating the distinction between thermodynamic products and kinetics-controlled products during materials preparation. (a) The free energy of two configurations as a function of thermodynamic parameters such as temperature, pressure, and applied potential bias. (b) Evolution of free energy during material processing.

thermodynamics defines the equilibrium atomic configuration of a solid material, the process that shapes this configuration is governed by kinetics. Under nonequilibrium conditions, the difference in free energy (ΔG) acts as the driving force for processes such as nucleation and crystal growth. The synthetic system thus finds a specific atomic configuration that occupies the minima in the free energy landscape, as depicted in Figure 1b. Both thermodynamic stable and metastable configurations exist within this landscape, corresponding to the global and regional minima, respectively. At either state, the composition and structure of the material are expected to remain stable, at least over the time scale of functioning. However, during synthesis, the material system may traverse a series of metastable states before reaching its final form. Analogous to chemical reactions, the selection of the final product is strongly influenced by kinetics. By exploiting the complex interplay between thermodynamics and kinetics,[29] researchers have successfully synthesized diverse materials with remarkable properties by kinetically trapping nonequilibrium states. In particular, imposing far-from-equilibrium conditions during synthesis enables the creation of unconventional materials with a large kinetics barrier (E_a), such as high-entropy nanomaterials and bulk-immiscible nanoalloys.

https://doi.org/10.1021/acsmaterialslett.4c01952
ACS Materials Lett. 2025, 7, 319−332

Far-from-equilibrium (FFE) is a concept relative to near-equilibrium. The thermodynamic state of a material system can be defined by the Gibbs free energy (G), which depends on enthalpy (H), entropy (S), and temperature (T) as given by $G = H - TS$. When an electric field is applied via a bias potential (ΔE), G can be expressed as $G = H - TS + nF\Delta E$. An FFE thermodynamic environment can be established by tuning its components in temporal or spatial dimensions, as depicted in Figure 2. The most direct approach is to change the temperature. For instance, a heat pulse rapidly stimulates the system to the thermodynamic state with substantial free energy change (ΔG), enabling capture of atomic configuration of a high temperature in a material system that contains several interplay processes with different kinetic features. This concept has been demonstrated by Hu's group in synthesizing high-entropy alloy nanoparticles through carbothermal shock methods.[26] Under a temporal FFE environment produced by pulse heating, high-entropy alloy nanoparticles containing 5−8 elements in an equimolar ratio[26] form, while their growth is inhibited. Similarly, a large spatial gradient of ΔG in space offers another route to facilitate a kinetics-dominant process for the synthesis and processing of materials by providing a large driving force. Detailed applications of FFE synthesis and processing, including Joule heating, millisecond pyrolysis, pulsed electrosynthesis, laser-assisted 3D printing, plasma electrolysis, and arc-discharging, are discussed in the following sections.

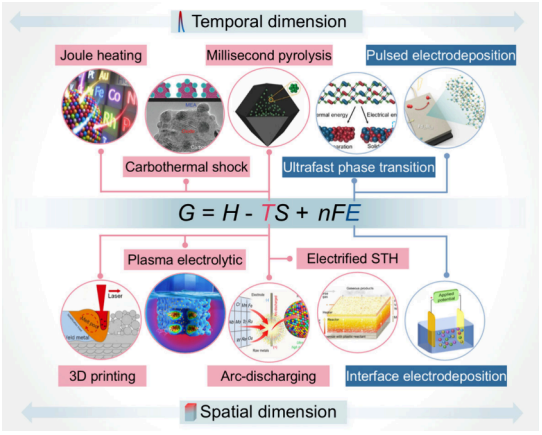

Figure 2. Schematic representation of far-form-equilibrium material synthesis regulated by thermodynamic parameters. *G* denotes the Gibbs free energy, *S* the entropy, *T* the temperature, *n* the number of electrons involved, *F* the Faraday constant, and *E* the applied voltage.

FFE STRATEGIES FOR SYNTHESIS AND PROCESSING

Temporal Regulation of Temperature (ΔT). Far-from-equilibrium processing subjects materials to conditions that deviate substantially from thermodynamic equilibrium, offering a distinctive pathway for creating novel materials with properties unattainable through conventional equilibrium-based methods.[14] Among the various thermodynamic parameters, temperature represents a fundamental one that significantly influences atomic interactions, dictating the stable structures and compositions of materials across different temperature regimes.[30] Even in conventional synthesis or processing of solid materials, precise control of temperature is of paramount importance.[31] The widespread adoption of high-temperature synthesis techniques has expanded the exploration of metastable materials. As illustrated in Figure 2, the key for FFE processing through temperature is to impose a significant temperature gradient in temporal and/or spatial dimensions so that a steep gradient in free energy can be realized. Following this principle, various processing strategies have been successfully developed.

In terms of temporal dimension, traditional near-equilibrium thermochemical methods exhibit relatively small temporal gradients, typically characterized by slower heating and cooling rates. In contrast, FFE techniques that employ substantial temperature gradients in time dimension, i.e., short-term pulse heating, can establish kinetic dominance and create the nonequilibrium thermodynamic conditions. Essentially, the pulsed heating provides significant thermodynamic driving forces while simultaneously restricting atomic diffusion, thereby facilitating the controlled fabrication of solid nanomaterials. Atomic diffusion, a thermally activated process, is described by the Arrhenius equation:

$$D = D_0 \exp\left(-\frac{\Delta H}{k_B T}\right) \quad (1)$$

where D is the diffusion coefficient, D_0 is the pre-exponential factor, ΔH is the activation enthalpy, k_B is the Boltzmann constant, and T is the temperature. According to the equation, atomic diffusion can be significantly suppressed by decreasing the temperature during processing. Consequently, achieving a kinetically controlled synthesis of solid nanomaterials requires confinement of atomic diffusion within extremely short timeframes.

Following the aforementioned principles, various fast-heating methods have been developed to fabricate materials of unique microstructures and compositions including both structural and functional materials. For tailoring the microstructure of steels and nonferrous alloys, techniques such as resistance heating, induction heating, and plasma discharge heating are employed,[32] as these methods can achieve a fast-heating rate greater than 100 °C s^{-1}. Due to the shortened time available for recovery and recrystallization, fast heating often results in a high density of dislocations, which contributes to increased alloy strength. Figure 3a illustrates this phenomenon by comparing the microstructure of an 80% cold-rolled 5052 aluminum alloy annealed at a slow rate (5 °C s^{-1}) and an ultrafast rate (500 °C s^{-1}).[33] Different from the uniform microstructure typically formed after conventional slow heating, ultrafast heating yields a nonequilibrium "soft-hard" microstructure, characterized by a mixture of substructured grains with high geometrically necessary dislocations and recrystallized grains with a low dislocation density at a ratio close to 1:1. The overlap of recovery and recrystallization phases during ultrafast heating is the primary reason for the formation of the unique mixed-grain microstructure, which contributes to increased strength while maintaining ductility of the Al-Mg alloy.

Another commonly observed effect of fast heating is grain refinement. Yuan et al. reported the refinement of parent austenite grains in low-carbon microalloyed steel by increasing the heating rate to 120 °C s^{-1}. This refinement was attributed to the reservation of (Nb, Ti, V)C precipitates and dislocations after a short heating period.[34] Similar refinement has also been

https://doi.org/10.1021/acsmaterialslett.4c01952
ACS Materials Lett. 2025, 7, 319−332

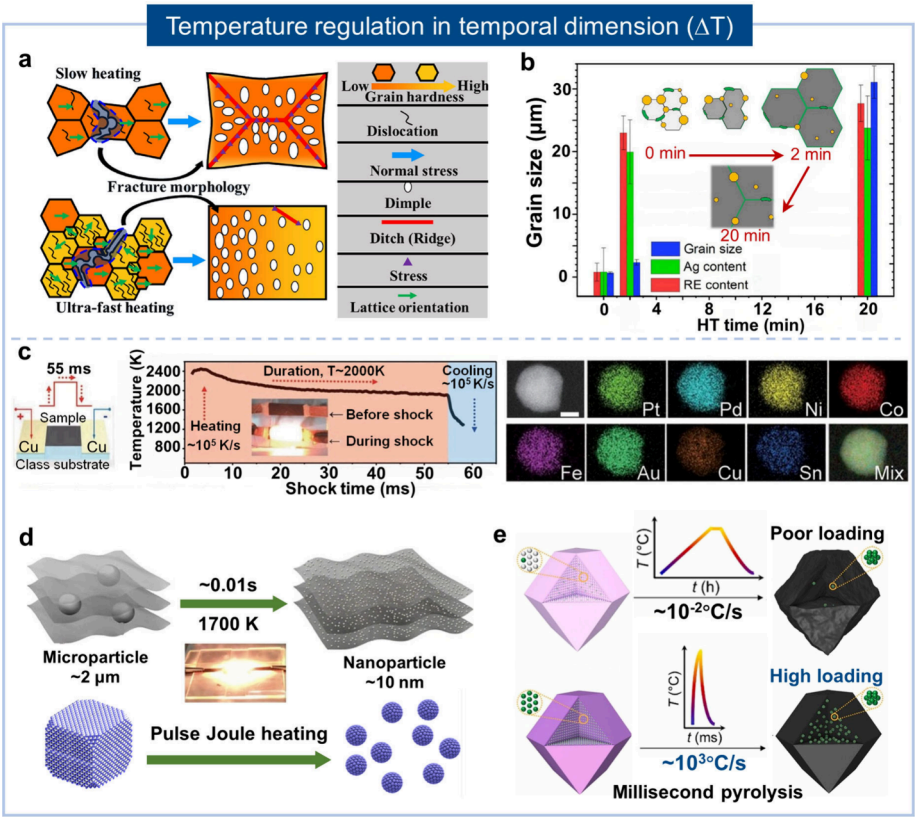

Figure 3. Far-form-equilibrium materials processing by manipulating temperature in the time dimension. (a) Microstructure of cold-rolled Al-Mg alloy after conventional slow heating and ultrafast heating treatment. The latter generates a mixture of hard grains with highly geometrically necessary dislocations and soft grains with low-density dislocations. Reproduced with permission from ref 33. Copyright 2024 Elsevier. (b) Evolution of grain size and solute element concentration in matrix of Mg-RE-Ag alloy as a function of heat treatment time. Reproduced with permission from ref 35. Copyright 2024 Elsevier. (c) Generation of thermal shock from a 55 ms current pulse and the corresponding temporal evolution of temperature for the preparation of HEA nanoparticles with uniform element distribution. Reproduced with permission from ref 26. Copyright 2018 American Association for the Advancement of Science. (d) Upper: Comparative schematic diagrams of synthesizing bimetallic nanoparticles using the far-from-equilibrium HTR method versus the near-equilibrium TFA method. Reproduced under the terms of the Creative Commons CC BY license from ref 39. Copyright 2016 Springer Nature. Lower: High-temperature pulse method for the redispersion of Pt NPs. Reproduced with permission from ref 40. Copyright 2020 American Chemical Society. (e) Influence of thermal pulse on synthesizing MOF-derived metal NPs. Reproduced with permission from ref 43. Copyright 2022 Elsevier.

observed in low-carbon low-alloy quenching and partitioning (Q&P) steels after ultrafast heating,[9] which delays the complete recrystallization of deformed ferrite and restrains tempering of deformed martensite. Consequently, the high-density residual deformation substructures enhance austenite nucleation by increasing the number of nucleation sites and promoting element partition. Fast heating also addresses the inherent contradiction between a high solute concentration and small grain size. Precipitation and grain refinement are two fundamental strengthening mechanisms in alloy materials that can be synergistically employed to maximize the strengthening effect. In Mg alloy, the high concentration of solute necessary for nanoprecipitation is often limited by solid solubility, as exemplified by Gd in the Mg matrix. To achieve a high degree of supersaturation of solutes in the matrix without excessive grain growth, Li et al. proposed a short-time heat treatment on Mg-RE-Ag alloys (where RE denotes rare earth elements).[35] As depicted in Figure 3b, the solute concentration of RE and Ag in the alloy matrix increases to 2.01% and 0.34%, respectively, after short-time heating, while grain growth remains limited compared to conventional heating.

The extreme temporal manipulation of the temperature is realized through pulse heating and cooling. In 2018, Hu and his colleagues introduced carbon thermal shock (CTS) technology as a general method for alloying multiple elements into high-entropy alloy (HEA) nanoparticles.[26] Briefly, a mixture of salt precursor MCl_xH_y (M = Pt, Pd, Ni, Fe, Co, Au, Cu, Sn, etc.) is initially loaded onto carbon nanofibers (CNFs). As shown in Figure 3c, flash heating (~10^5 °C s^{-1}) to about 2000 K is applied to the CNF substrate for 55 ms using an electric pulse, followed by rapid cooling (~10^5 °C s^{-1}). This method leverages the high temperatures and rapid cooling to drive rapid mixing and solidification of multiple metallic elements that would otherwise be immiscible, resulting in HEA nanoparticles up to eight elements with uniform distribution. The fast heating/cooling method has been extended to the synthesis of quinary high-entropy oxide.[36] A homogeneous precursor containing several metal chlorides was rapidly added into sodium nitrate ionic melt at 350 °C, followed by fast cooling to yield high-entropy oxide ($RuIrFeCoNiO_2$) nanoparticles.[36] The rapid cooling promotes nuclei formation with a random orientation distribution and suppresses crystal growth.

https://doi.org/10.1021/acsmaterialslett.4c01952
ACS Materials Lett. 2025, 7, 319−332

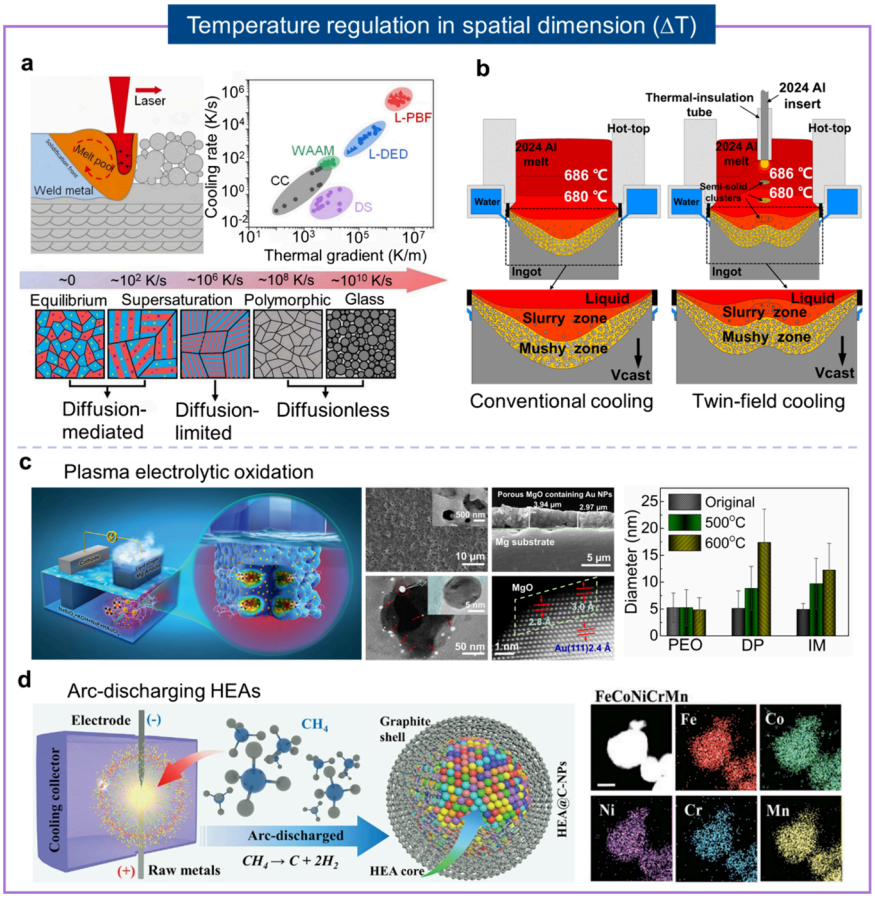

Figure 4. Far-from-equilibrium materials obtained by controlling temperature (ΔT) on a spatial scale. (a) Temperature field within 3D-printed materials during processing and the resulting highly metastable microstructure of multicomponent eutectic alloys. Reproduced with permission from ref 44. Copyright 2022 Springer Nature. (b) Comparison of direct cooling and twin-cooling field solidification techniques along with their respective microstructures. Reproduced with permission from ref 48. Copyright 2022 Elsevier. (c) The *in situ* preparation of the hierarchical structured Au/MgO catalyst on a Mg substrate by an instant high-temperature interfacial plasma electrolytic oxidation process. Reproduced with permission from ref 50. Copyright 2019 Royal Society of Chemistry. (d) Schematic of the arc-discharged approach for synthesizing HEA-NPs. Reproduced with permission from ref 55. Copyright 2022 Wiley.

As a result, the obtained $RuIrFeCoNiO_2$ nanoparticles have abundant grain boundaries that enhance catalytic activity.

Following Hu's pioneering work, various methods to generate high temperature pulse have been developed, including Joule heating, laser heating, and microwave treatment.[37,38] And the application has been extended beyond the preparation of metastable nanomaterials to include solid waste treatment, the evaporation of precious metals, and ceramic sintering. Chen et al.[39] report that uniformly distributed nanoparticles with a diameter of about 10 nm can self-assemble on a reduced graphene oxide matrix in just 10 ms (Figure 3d). More importantly, high-temperature pulse treatment could transform large aggregated particles into nanoscale materials.[40] By applying a thermal shock (~1500−2000 K) for a very short time (100 ms) followed by rapid quenching back to room temperature at 10^5 K/s, micrometer-sized metal oxide particles are redispersed into metallic nanoparticles of ~10 nm in size. This counterintuitive change in particle size reflects the distinct nature of far-from-equilibrium processing. The advantage of FFE synthesis has been demonstrated by comparing with the traditional tube furnace annealing (TFA) method that is difficult to balance particle size, dispersion, and grain coarsening.[41] It was found that the FFE ultrafast high-temperature irradiation (HTR) method enables the fabrication of ultrafine bimetallic alloy nanoparticles with a narrow size distribution (~10−20 nm) and uniform dispersion.

A high-performance catalyst requires not only exceptional intrinsic activity at the reactive sites but also a high loading density. Therefore, synthesizing supported catalysts with an elevated loading content is paramount. However, agglomeration often occurs when increasing the number of nanoparticles supported on a specific substrate.[42] To overcome this limitation, FFE methods have been applied to prepare supported nanocatalysts, achieving both high metal loading and ultrasmall size simultaneously. Figure 3e illustrates the utilization of millisecond pyrolysis technology to trade-off ultrasmall size and high loading in metal−organic framework-derived metal nanoparticles.[43] Through rapid pyrolysis of MOFs (at ~1000 °C within 0.3 s), controlled synthesis of metastable ultrasmall non-noble metal nanoparticles (NPs) is accomplished. In this process, the rapid pyrolysis under FFE conditions induces only the initial nucleation, preventing Ostwald ripening or further coalescence, thereby enabling the creation of innovative FFE materials with a high metal loading and ultrasmall size. Using carbon nanofiber film as a heater, the high treatment temperature (~1500−2000 K) is quickly reached and maintained for a very brief duration (100 ms), followed by rapid quenching to room temperature to impede

https://doi.org/10.1021/acsmaterialslett.4c01952
ACS Materials Lett. 2025, 7, 319−332

sintering.[40] Under such FFE conditions, large aggregated metal oxide particles were dispersed into uniformly distributed metallic nanoparticles on the substrate. In contrast to conventional near-equilibrium redispersion treatments, this method yields superior particle dispersion, smaller sizes, and a significantly faster preparation speed.

Spatial Regulation of Temperature (ΔT). In most materials processing techniques, materials are heated to high temperatures by using external energy sources such as radiation, convection, or conduction. This often creates a spatial temperature gradient within the material due to a mismatch between the energy source and the heated region. When the temperature gradient is sufficiently large, it establishes a far-from-equilibrium environment for the constituent atoms, enabling the formation of unconventional microstructures by tuning the relative kinetics of dependent processes, such as atomic diffusion, grain growth, and element alloying.

In the field of structural materials, two typical examples of materials processing under large temperature gradients are additive manufacturing[44] and surface strengthening treatment.[45] The former fabricates components via a layer-by-layer strategy, where a thin layer of metal powders is spread on a solid metal substrate and then selectively melted by a laser or electron beam,[46] as schematically illustrated in Figure 4a. The melted alloy can reach high temperatures exceeding 2000 K in localized areas, resulting in a large temperature gradient.[47] It is important to note that the spatial gradient of temperature is linearly correlated to a cooling rate for additive manufacturing processes, including laser powder bed fusion (L-PBF), laser directed energy deposition (L-DED), wire arc additive manufacturing (WAAM), conventional casting (CC), and directional solidification (DS).[44] L-PBF, the most prevalent metal additive manufacturing technique, exhibits extremely high cooling rates and thermal gradients. Therefore, a unique type of far-from-equilibrium microstructure in the form of dual-phase nanolamellae embedded in eutectic colonies in an $AlCoCrFeNi_{2.1}$ eutectic HEA is produced through diffusion-limited solidification in the L-PBF process.

However, it should be noted that a large temperature gradient can, in some cases, be detrimental to the formation of the desired microstructures. For instance, coarse-grained dendritic microstructures and negative segregation are frequently observed in cast alloys, limiting the performance of downstream products. This is primarily attributed to the low cooling rate imposed by thermal conductivity, which maintains the interior of the material at a relatively high temperature for extended periods. To address the issue, Qin et al.[48] proposed the concept of twin-cold field for casting. The core principle involves immersing an alloy rod of the same composition as the ingot into the melt along the central axis of a hot-top. The immersed rod acts as a "cold source" that dissipates the latent heat of solidification at the center of the ingot. Thus, the equilibrium conditions controlling dendrite formation during solidification is disrupted. As shown in Figure 4b, the curvature of the liquid/solid interface is noticeably reduced by the immersed cold rod, which is beneficial for refining crystal grains. By applying this concept to the casting of 2024 Al alloy, the average grain size at the ingot center was decreased by 40% to 721 μm compared to conventional casting due to an increase in nucleation sites. And homogeneity of the grain size along the radical direction is significantly improved.

A steep temperature gradient can be established at the solid−liquid interface by imposing a large voltage (generally exceeding 100 V) to induce discharging, particularly on the surface of valve metals, such as Mg, Al, and Ti. Plasma electrolytic oxidation (PEO), based on the discharging phenomena, is widely used to prepare inorganic protective layers on these metals.[49] Recently, Li and Qin extended this method to fabricate structured catalysts composed of mesoporous oxide-supported nanometals.[50] Figure 4c illustrates the growth of the Au/MgO catalyst layer on the Mg substrate. Briefly, a magnesium plate and a stainless-steel plate are placed in an electrolyte containing precursor salt ($HAuCl_4$), acting as the anode and cathode, respectively. Shortly after application of a high voltage, the Mg surface is heated to an extremely high temperature, facilitating the decomposition of the precursors and forming Au NPs encapsulated in porous MgO. The temperature gradient at the interface can be intensified further by cooling the system with liquid nitrogen. As a result, a reactive and far-from-equilibrium environment is setup, decreasing the average size of deposited Au nanoparticles from 6.9 to 2.9 nm.[50] The Au/MgO catalyst prepared by this interfacial PEO method exhibits exceptional high thermal stability due to the anchoring effect of abundant oxygen vacancies.[42] Using this method, a variety of structured catalysts, including Ru, Pd, Pt, and their alloys, have been prepared on the bulk surfaces of Ti and Mg.[51]

Arc discharge between two electrodes also generates thermodynamic states far-from-equilibrium by applying high voltage (Figure 4d).[52] This technique was initially developed for synthesizing carbon nanotubes (CNTs) and has since been extended to a broad range of carbon-based materials. Arc discharge synthesis is typically conducted within a chamber utilizing two electrodes. One packed with a carbon precursor packed with a metal catalyst is usually used as the anode, while the other, the cathode, is made of pure graphite. The arc current generates plasma at a very high temperature of ∼4000−6000 K, vaporizing the carbon precursor and catalyst. The resulting carbon vapor, along with the catalyst particles, condenses on the cooler cathode or chamber walls, forming CNTs.[53] Heteroatom-doped carbon materials can be prepared by introducing doping elements into the chamber gas or into the anode as a filler. Kim et al. enhanced the doping efficiency in N-doped graphene through arc discharge by incorporating polyaniline as anodic carbon fillers, achieving a high doping level of ∼3.5% while maintaining high crystallinity.[54] Owning to the FFE nature of the arc discharge, high-entropy nanoparticles with a graphite shell (HEA@C-NPs) have been prepared. As shown in Figure 4d, the core−shell structure was formed by arc-discharging a cylindric target comprised of high-entropy alloys in a flow of methane and argon (CH_4:Ar = 2:1).[55] By adjusting the cooling rate and vapor pressure in the chamber, composite supermixed nanoparticles consisting of up to 21 elements were synthesized.[52]

Electrochemical Regulation. In electrochemical processes, the thermodynamic conditions of the synthesis system can be significantly and promptly altered by adjusting the electrode potential, as described by the Nernst equation $\Delta G = -nFE$ (n is the number of electrons involved, F is the Faraday constant, and E is the cell potential). In this context, the electrode potential in electrochemical processes plays a role analogous to that of temperature in thermal activation-controlled growth kinetics. Noting the change in Gibbs free

https://doi.org/10.1021/acsmaterialslett.4c01952
ACS Materials Lett. 2025, 7, 319−332

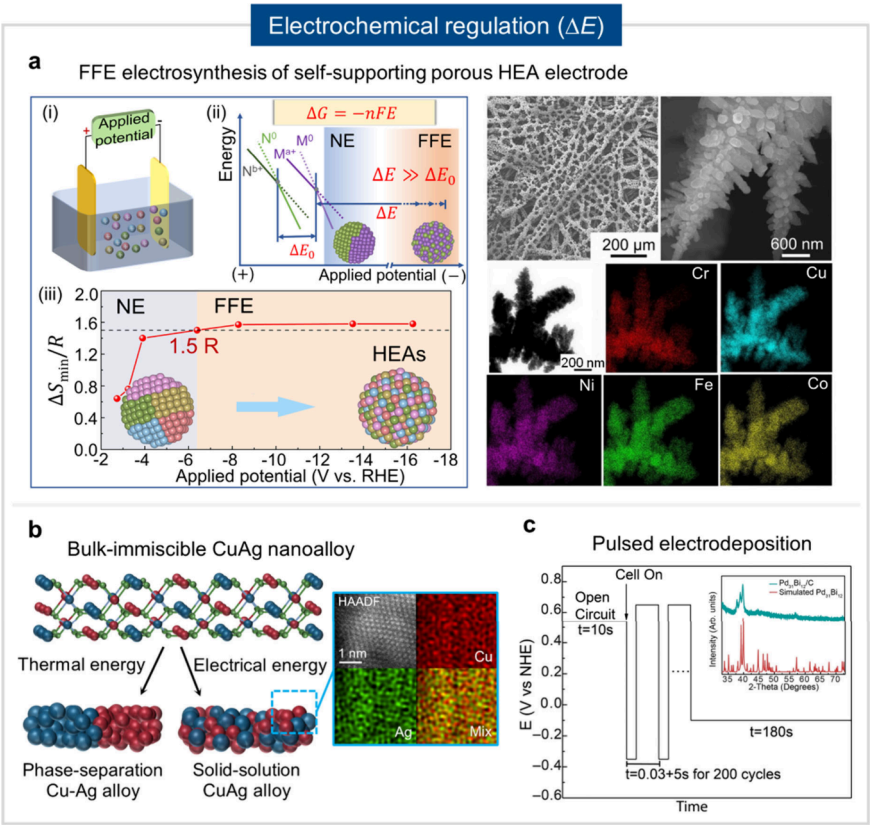

Figure 5. Far-from-equilibrium materials obtained by controlling voltage (Δ*E*). (a) Illustration of far-from-equilibrium electrosynthesis showcasing the preparation and characterization of FeCoNiCrCu HEAs. Reproduced with permission from ref 56. Copyright 2023 Elsevier. (b) Solid-solution CuAg alloy prepared by electrochemical starting from the parent oxide. Reproduced with permission from ref 57. Copyright 2022 Royal Society of Chemistry. (c) Pulsed electrodeposition of metastable $Pd_{31}Bi_{12}$ nanoparticles. Reproduced with permission from ref 58. Copyright 2020 American Chemical Society.

energy (ΔG) can easily be induced by electrode potential at the eV level, which is much larger than thermal energy at room temperature (k_BT, ~25 meV), it is convenient to create an FFE environment by regulating the electrode potential. In thermal chemistry, especially through high-temperature pulse techniques, the initiation and subsequent quenching of heat pulses involve intricate processes of energy conversion, transfer, and dissipation. The regulation of heat treatment over temporal scales (seconds or submilliseconds) heavily depends on factors such as thermal conductivity, specific heat capacity, and reactor design. In comparison, electrochemical methods allow for the regulation of Gibbs free energy (ΔG) by simply applying a potential bias (E) to the electrode.

Conventional electrochemical deposition of alloy nanostructures is typically conducted at mild potentials that are cathodic to but not significantly distant from the standard reduction potential (E_0) of the constituent elements. Under these conditions, phase separation frequently occurs rather than the formation of alloys with uniform element distribution. To fabricate hierarchical nanostructures of high-entropy alloys (HEAs), we recently proposed a far-from-equilibrium electrosynthesis strategy.[56] As shown in Figure 5a, alloys are electrodeposited from an electrolyte containing multiple metal precursors (e.g., chlorides of Cr, Fe, Co, Ni, and Cu). A strong correlation between the configuration entropy (ΔS_{mix}) of the alloy and the applied potential was found. At a high potential of 6.4 V, the ΔS_{mix} of the synthesized alloy surpasses the criterion for HEA (1.5R). The synthesized HEAs exhibit a uniform element distribution, even at the atomic scale, indicating that the disparity in reduction potentials among the multiple metals has been effectively mitigated (i.e., $E_a \gg E_0$) under FFE conditions. Moreover, these HEAs have a hierarchically porous structure, making them suitable for electrocatalytic applications. This FFE electrosynthesis strategy holds general significance, as it represents a general approach for fabricating self-supporting HEA electrodes.

Electrochemical processes enable the fabrication of metastable materials that are often unattainable through thermochemical methods. A notable class of metastable materials is bulk-immiscible nanoalloys, which tend to phase-separate into distinct components under equilibrium conditions due to their immiscibility in their bulk form. These nanoalloys frequently exhibit enhanced catalytic activity or mechanical strength. For instance, tandem catalysis, which involves catalytic roles of two distinct sites, is an effective strategy to circumvent the limitations imposed by the linear scaling relationship in electrocatalytic CO_2-to-C_2H_4.[59] While Ag and Cu are efficient in forming *CO intermediates and dimerization of *CO, respectively, synthesizing CuAg nanoalloys with random and uniform distribution remains challenging due to the inherent immiscibility at ambient temperatures. Figure 5b illustrates FFE electrosynthesis of solid-solution CuAg nanoalloy starting from the parent oxide $Ag_2Cu_2O_3$.[57] By subjecting the $Ag_2Cu_2O_3$ nanorods to a large cathodic potential, significantly exceeding the standard reduction potentials of Cu^{2+}/Cu^0 and Ag^+/Ag^0, the FFE environment enables the simultaneous and

https://doi.org/10.1021/acsmaterialslett.4c01952
ACS Materials Lett. 2025, 7, 319−332

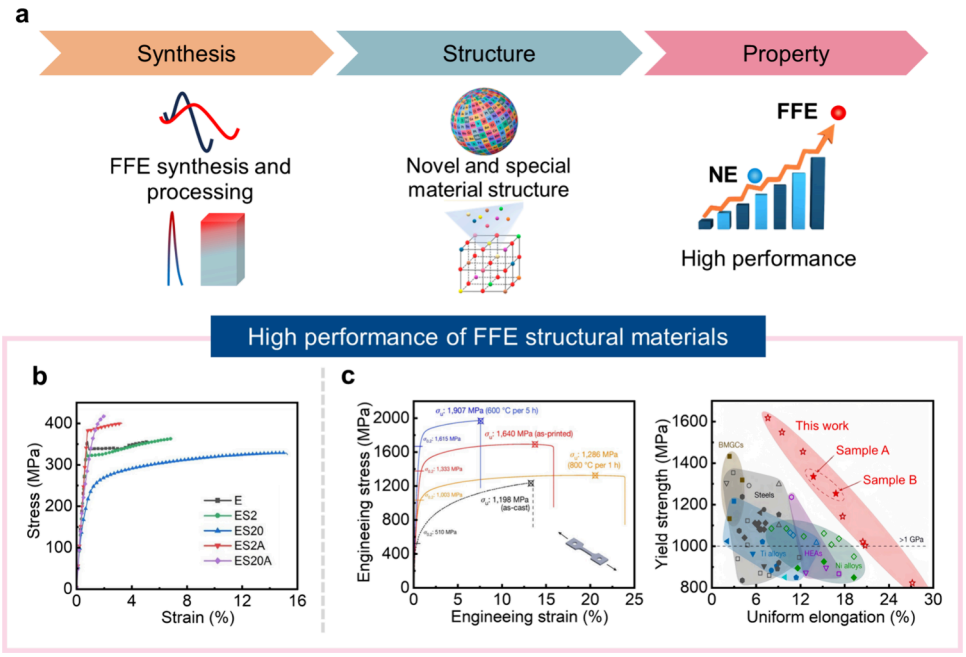

Figure 6. Unique properties of far-from-equilibrium structural materials. (a) Schematic diagram illustrating the synthesis-structure−property relationship of FFE materials. (b) Tensile engineering stress−strain curves of E, ES2, ES20, ES2A, and ES20A samples. Reproduced with permission from ref 35. Copyright 2024 Elsevier. (c) Tensile properties of AM $AlCoCrFeNi_{2.1}$ EHEAs and its comparison with other materials. Reproduced with permission from ref 44. Copyright 2022 Springer Nature.

rapid reduction of Cu and Ag cations within $Ag_2Cu_2O_3$. Moreover, limited atomic diffusion at mild temperatures ensures mixing of Cu and Ag at the atomic scale. As revealed by energy dispersive spectroscopy (EDS) mapping, Cu and Ag atoms are uniformly distributed in the electrosynthesized CuAg nanoalloy.

In solid-solution alloys, metal atoms are generally randomly distributed within the lattice, imposing constraints on the precise manipulation of the microenvironment of reactive centers. In contrast, constituent atoms are periodically arranged by strong ionic and/or electronic interactions in ordered intermetallic compounds, bridging the gap between traditional metal nanocatalysts and the single-atom catalysts.[60] Hall et al. developed a FFE method through pulsed electrodeposition at room temperature for synthesizing metastable ordered intermetallic $Pd_{31}Bi_{12}$ nanoparticles.[58] As shown in Figure 5c, a pulsed potentiation waveform at a large overpotential was applied to initiate uniform nucleation on a carbon substrate followed by constant-potential deposition to grow the deposited nuclei. The applied potential (−0.35 V vs NHE) is higher than the minimum potential needed to deposit Pd or Pd-Bi alloys, facilitating access to the nonequilibrium environment. The synthesized $Pd_{31}Bi_{12}$ nanoparticles exhibit a surface area of ∼37 m^2/g, nearly 40 times greater than that of the low-porosity thin film generated by conventional electrodeposition processes.

UNIQUE PERFORMANCE OF FFE MATERIALS

The performance of materials is intricately linked to their structures. Far-from-equilibrium materials, synthesized in extreme environments, exhibit distinctive structures that deviate significantly from those of conventional materials. Consequently, these unconventional structures have opened the door to unique functionalities (Figure 6a). This section focuses on how materials prepared via far-from-equilibrium processes exhibit remarkable performance due to their unique structures, including both structural and functional materials.

For structural materials, FFE processing provides a feasible route to reach breakthrough mechanical properties by the formation of unprecedented microstructures. For example, alloys produced through rapid solidification demonstrate exceptional mechanical strength due to their extremely small grain sizes. An extremely short heat treatment (ESHT) generated an ultrafine-grained, weakly textured Mg-RE-Ag extruded alloy with numerous dynamic precipitates (Figure 6b).[35] The FFE process greatly increased the concentration of the main solutes in the matrix, promoting precipitation of nanoprecipitates (prismatic β' and basal γ'') without excessive grain growth. The precipitation hardening response (ΔH_V = 37.2 HV) and yield strength were significantly enhanced.

Moreover, FFE methods are used to enhance the impact resistance and thermal stability of composite materials with layered or gradient structures. Dual-phase nanolamellar high-entropy alloys (HEAs) were manufactured using large temperature gradient and rapid cooling, exhibiting high yield strength (Figure 6c).[44] The high strength arises from the alternating face-centered cubic and body-centered cubic nanolayers that formed during far-from-equilibrium processing. The laser powder bed fusion (L-PBF) manufactured $AlCoCrFeNi_{2.1}$ HEAs demonstrated a high yield strength of about 1.3 GPa and a substantial uniform elongation of about 14%,[44] surpassing other state-of-the-art additively manufactured metal alloys. The far-from-equilibrium characteristics during 3D printing provide mechanistic insights into the deformation behavior of the fabricated HEAs components, which are crucial for developing alloys with exceptional mechanical properties.

For functional nanomaterials, synthesis under FFE conditions not only affects the size and shape of the materials but also allows for the precise control of their chemical

https://doi.org/10.1021/acsmaterialslett.4c01952
ACS Materials Lett. 2025, 7, 319−332

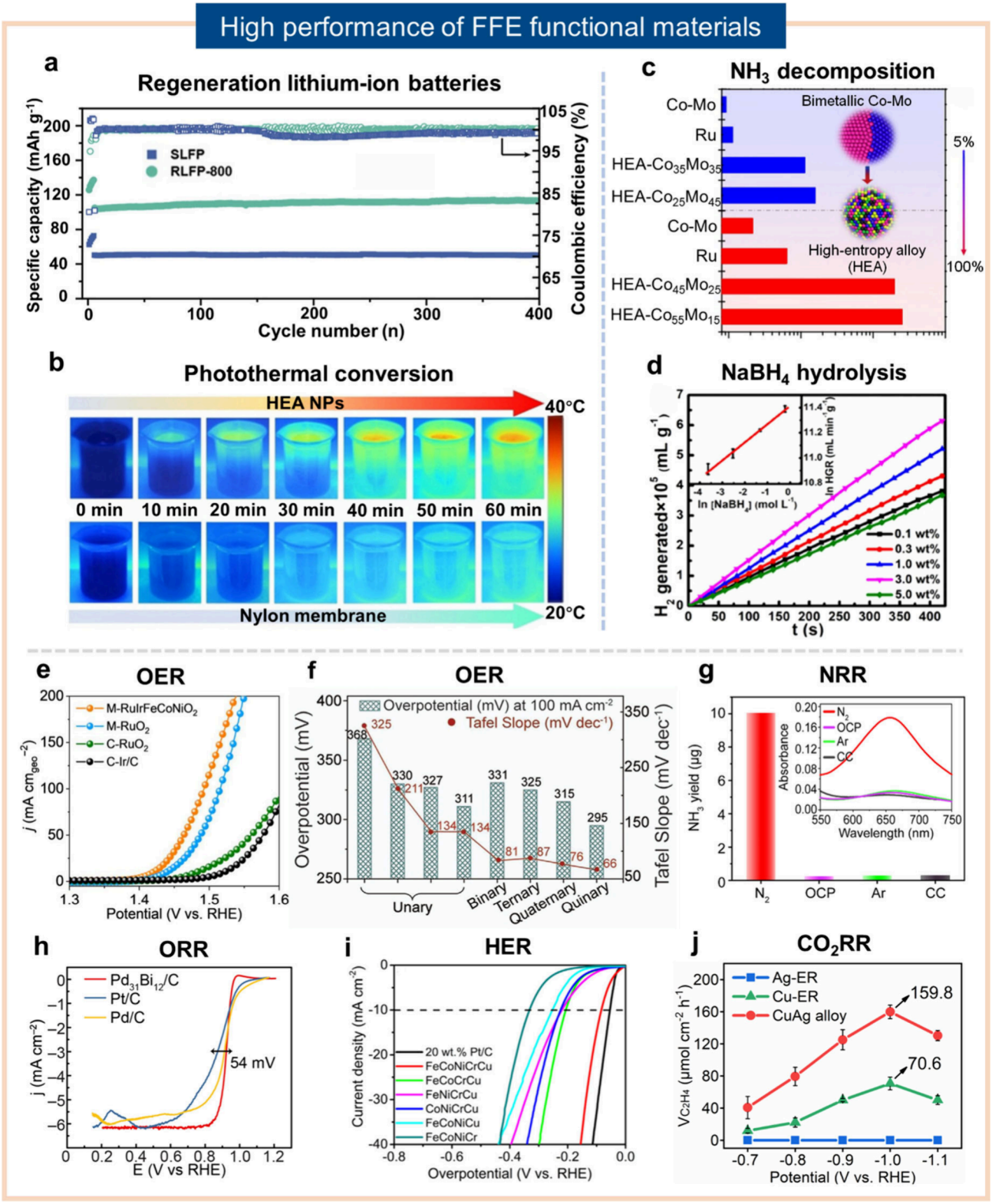

Figure 7. Unique properties of far-from-equilibrium functional materials. (a) Regenerated $LiFePO_4$ cathode demonstrating long cycling stability. Reproduced with permission from ref 62. Copyright 2023 Elsevier. (b) Photothermal conversion effect observed in a nylon membrane evaporator with and without septenary HEA NPs exposed to 1 sun solar radiation for 60 min. Reproduced with permission from ref 63. Copyright 2021 Wiley. (c) The performance of HEA-Co_xMo_y nanoparticles in ammonia decomposition at varying concentrations. Reproduced under the terms of the Creative Commons CC BY license from ref 67. Copyright 2019 Springer Nature. (d) The effective application of the Ru/MgO catalyst grown in situ on a magnesium substrate in the hydrolysis of sodium borohydride to produce hydrogen. Reproduced with permission from ref 51. Copyright 2021 American Chemical Society. (e) Electrocatalytic OER properties of M-$RuIrFeCoNiO_2$ and control catalysts in 0.5 M H_2SO_4. Reproduced with permission from ref 36. Copyright 2023 American Association for the Advancement of Science. (f) Performance of various M_xS_y as electrocatalysts for OER. Reproduced with permission from ref 68.

https://doi.org/10.1021/acsmaterialslett.4c01952
ACS Materials Lett. 2025, 7, 319−332

Figure 7. continued

Copyright 2021 Wiley. (g) Nitrogen reduction reaction (NRR) performance of MOF-derived ultrasmall NPs. Reproduced with permission from ref 43. Copyright 2022 Elsevier. (h) Electrocatalytic oxygen reduction reaction (ORR) performance of metastable $Pd_{31}Bi_{12}$ nanoparticles. Reproduced with permission from ref 58. Copyright 2020 American Chemical Society. (i) Hydrogen evolution reaction (HER) performance of high-entropy alloy samples. Reproduced with permission from ref 56. Copyright 2023 Elsevier. (j) Electrocatalytic carbon dioxide reduction (CO_2RR) of the solid-solution CuAg alloy. Reproduced with permission from ref 57. Copyright 2022 Royal Society of Chemistry.

composition and electronic structure. Bimetallic alloy nanomaterials, exhibiting superior electrochemical performance, are emerging as promising anode materials for batteries.[41] By employing a rapid high-temperature radiance (HTR) FFE technique, a series of ultrafine bimetallic alloys was synthesized, characterized by a narrow size distribution (∼10−20 nm), uniform dispersion, and high loading capacities. These unique structural features confer exceptional stability to the BiSb-HTR anode, which shows negligible degradation even after 800 cycles. This FFE approach can rapidly fabricate a variety of bimetallic nanoalloys, thereby having broad potential applications in energy storage, energy conversion, and electrocatalysis.[61]

The demand for lithium-ion batteries (LIBs) has surged due to advancement in energy storage; however, this has also led to a significant number of spent batteries, making their recovery an urgent task. Traditional regeneration methods typically rely on near-equilibrium techniques, which are time-consuming and energy-intensive. Wu et al. proposed an efficient, low-cost, and ultrafast regeneration strategy under FFE conditions, requiring only 20 s to regenerate spent $LiFePO_4$ (LFP) (Figure 7a).[62] It achieves complete lithium replenishment and structure repair of $LiFePO_4$, recovering an initial capacity of 152 mAh g^{-1} and cycling stability.

FeCoNiTiVCrCu HEA nanoparticles synthesized via the arc-discharge FFE method demonstrated high proficiency in photothermal conversion (Figure 7b).[63] Because energy levels both below and above the Fermi level (∼4 eV) are entirely occupied by 3d transition metals, the HEA achieves a high light absorption exceeding 96% across a broad solar spectrum between 250 and 2500 nm. Correspondingly, the absorbed solar irradiation is efficiently converted into heat on the surface, enabling a solar steam generator based on the HEA nanoparticles to achieve a photothermal conversion efficiency above 98% and a high evaporation rate of 2.26 kg m^{-2} h^{-1}.

Heterogeneous catalysts are crucial for building a sustainable society and represent a frontier in materials research. The intrinsic activity of a heterogeneous catalyst depends on the local atomic and thus electronic structure of active sites. FFE materials with unconventional structures are expected to exhibit remarkable catalytic properties. Figure 7c−i illustrates their catalytic applications in important energy reactions, including water splitting, nitrogen fixation, and fuel cells.[26,36,43,50,51,56,57,63,64] The distinctive structural attributes of FFE materials enhance interactions between reactants and catalysts, consequently augmenting catalytic performance.[65] In intricate solid-solution materials, the formation of numerous diverse multielement active sites has introduced a novel and distinctive catalyst design concept that alleviates existing constraints.[66] Studies have shown that novel high-entropy alloy (HEA) catalysts synthesized under FFE conditions exhibit noteworthy efficiency in ammonia decomposition (Figure 7c).[67] HEA nanoparticles display significantly increased catalytic activity and sustained stability during ammonia decomposition. The tuning of their catalytic activity involves adjusting the Co/Mo ratio to optimize surface properties, thereby maximizing the reactivity across diverse reaction conditions.

A structured catalyst possessing switchable characteristics was developed by cultivating a nano Ru-embedded MgO coating on a magnesium substrate through an instantaneous high-temperature plasma oxidation process. The obtained Ru/MgO/Mg catalyst is effective for the hydrolysis of sodium borohydride ($NaBH_4$) (Figure 7d).[50,51] The high activity observed during $NaBH_4$ hydrolysis is attributed to the porous MgO framework formed during the FFE preparation process and the monodisperse Ru NPs with ultrasmall particle size. This configuration provides an optimal environment for reactant entry and mass transport, facilitating reaction initiation and the expulsion of byproducts to prevent catalyst poisoning.

Furthermore, Figure 7e showcases the oxygen evolution reaction (OER) performance of a quinary high-entropy ruthenium−iridium-based oxide (M-RuIrFeCoNiO_2) in 0.5 M H_2SO_4,[36] illustrating a low overpotential of 189 mV at 10 mA cm^{-2}. The grain boundaries generated under thermodynamically extreme conditions play a pivotal role in enhancing the OER activity and stability. In addition to high-entropy alloy oxides, transition metal sulfides with multielemental characteristics are also suggested as a promising class of catalysts for the oxygen evolution reaction (OER). Cui et al. synthesized high-entropy metal sulfides (HEMS, i.e., (CrMnFeCoNi)S_x) nanoparticles using the Joule heating method. Compared to unary, binary, ternary, and quaternary sulfides, the (CrMnFeCoNi)S_x catalyst demonstrated excellent OER activity and good durability (Figure 7f).[68] Meanwhile, high metal-loaded and ultrasmall-sized metal−organic framework (MOFs) materials, achieved through ultrashort pulse FFE conditions, are employed for N_2 electroreduction (NRR) (Figure 7g).[69] The resulting CoPd NPs@NCF catalyst exhibits notable activity and stability during the prolonged NRR catalytic reactions.

Through the utilization of pulsed electrochemical deposition, metastable ordered intermetallic compound $Pd_{31}Bi_{12}$ nanoparticles, when suspended on a carbon carrier, demonstrate outstanding performance in both the oxygen reduction reaction (ORR) and the tolerance to methanol during oxygen reduction (Figure 7h).[58] The application of a substantial electrochemical overpotential can create FFE conditions, enabling the synthesis of novel hierarchical and self-supporting nanostructures of high-entropy alloys (HEAs).[56] These nanostructures serve as electrocatalysts for the hydrogen evolution reaction (HER) in alkaline media, exhibiting low overpotentials and high catalytic activity (Figure 7i). While combining Cu and Ag into an alloy state holds promise as a tandem catalyst for electrocatalytic CO_2 reduction (CO_2RR),[57] challenges arise due to their immiscibility in the bulk. To address this issue, an FFE electrochemical synthesis method

https://doi.org/10.1021/acsmaterialslett.4c01952
ACS Materials Lett. 2025, 7, 319−332

was utilized to prepare the solid solution of the CuAg alloy. The CuAg nanoalloy achieves a high formation rate of C_2H_4 at 159.8 μmol cm^{-1} h^{-1}, which is 2.3 times higher than that on Cu alone (Figure 7g). In summary, far-from-equilibrium materials exhibit distinctive properties, demonstrating substantial promise for diverse applications.

In summary, conventional near-equilibrium material processing has imposed significant limitations on the customization of microstructures and properties of materials. Far-from-equilibrium methods represent a paradigm shift, overcoming thermodynamic limitations on material growth kinetics and unlocking new possibilities for materials design. In this review, we focus on principles and application of applying an FFE environment through temperature and potential to regulate system free energy (ΔG). Particularly noteworthy is the substantial impact of extreme voltages (ΔE) on thermodynamic parameters, bridging the gap in synthesizing FFE materials solely through thermochemical methods (ΔT). Despite significant advancements, research on far-from-equilibrium synthesis and materials remains in its early stages. Numerous scientific and technological challenges necessitate attention and resolution, particularly in the following areas.

Precise Control of Far-from-Equilibrium Processes. FFE processes often involve rapid evolution of materials structures within very short timeframes. Precise control over parameters like temperature, pressure, voltage, and time is essential for intentionally tuning microstructures and the desired properties. Improved process control also enhances the reproducibility of the synthesis. To achieve this goal, novel FFE processing strategies that can synergistically adjust multiple thermodynamic parameters should be developed.

Electrification of FFE Processes. Currently, FFE synthesis or processing is mainly operated by controlling temperature in the temporal-spatial dimensions. Electrochemical manipulation through voltage or potential provides an efficient route to tune the systems thermodynamics. Compared with temperature regulation, electrified FFE methods have advantages including fast response, substantial changes in free energy, and ease of operation. Integrating electric parameters into FFE processes not only introduces additional control but also fosters a more comprehensive understanding of material behaviors in nonequilibrium conditions. This endeavor contributes significantly to advancing the field of materials science.

Stabilization of FFE Synthesized Materials. Materials prepared through FFE methods are typically metastable from a thermodynamic perspective. Their unique structures might undergo changes under external influences or specific environments, potentially degrading their performance. Therefore, enhancing the stability of FFE materials, in terms of both structure and function performance, should be a priority in research efforts. In addition, the evolution of materials under long-term functioning conditions, including structure and properties, should be investigated.

Integration with AI-Powered Data Science. As a revolutionary tool in fundamental research, AI-powered data science can accelerate materials discovery and the development of novel synthesis methods. By employing machine learning methodologies, researchers can analyze vast data sets generated from FFE experiments, identifying correlations among process parameters, material properties, and microstructures, enabling a profound understanding of FFE processing and materials. In addition, AI-powered predictive modeling can be used to explore new FFE regimes, reducing the need for costly trial-and-error approaches. The integration of data science is expected to accelerate research on FFE processing and materials.

Novel Applications of FFE Materials. The atomic configuration and microstructure features of FFE materials are significantly distinct from those of conventional materials synthesized under near-equilibrium conditions. This expansion of materials brings opportunities to verify the existing structure−property relationship established for convention materials. Moreover, FFE materials may exhibit outstanding performance and novel properties, providing potential solutions to pressing challenges in energy, catalysis, and other fields.

By addressing these challenges, future research on FFE synthesis and materials can unlock even greater potential for the development of novel materials with exceptional properties and diverse applications.

AUTHOR INFORMATION

Corresponding Author

Song Li − *Key Lab for Anisotropy and Texture of Materials (MoE), School of Materials Science and Engineering, Northeastern University, Shenyang 110819, China;* orcid.org/0000-0002-9140-9973; Email: lis@atm.neu.edu.cn

Authors

Yihong Yu − *Key Lab for Anisotropy and Texture of Materials (MoE), School of Materials Science and Engineering, Northeastern University, Shenyang 110819, China*

Zhengpeng Qin − *Key Lab for Anisotropy and Texture of Materials (MoE), School of Materials Science and Engineering, Northeastern University, Shenyang 110819, China*

Xuefeng Zhang − *Institute of Advanced Magnetic Materials, College of Materials and Environmental Engineering, Hangzhou Dianzi University, Hangzhou 310012, China*

Yanan Chen − *School of Materials Science and Engineering, Tianjin University, Tianjin 300072, China;* orcid.org/0000-0002-6346-6372

Gaowu Qin − *Key Lab for Anisotropy and Texture of Materials (MoE), School of Materials Science and Engineering, Northeastern University, Shenyang 110819, China; Institute for Materials Intelligent Technology, Liaoning Academy of Materials, Shenyang 110010, China*

Complete contact information is available at: https://pubs.acs.org/10.1021/acsmaterialslett.4c01952

Author Contributions

CRediT: **Yihong Yu**: Conceptualization, writing - original draft. **Zhengpeng Qin**: Writing-review and editing. **Xuefeng Zhang**: Writing-review and editing. **Yanan Chen**: Writing-review and editing. **Gaowu Qin**: Writing-review and editing, Supervision. **Song Li**: Writing-review and editing, Supervision, Funding acquisition, Conceptualization.

Notes

The authors declare no competing financial interest.

ACKNOWLEDGMENTS

This work was funded by the National Natural Science Foundation of China (U23A20545, 52331001), the China

BaoWu Low Carbon Metallurgy Innovation Foundation-BWLCF202113, the Fundamental Research Funds for the Central Universities (N2202012), and the Science Foundation of Liaoning Province.

REFERENCES

(1) Chu, S.; Cui, Y.; Liu, N. The Path towards Sustainable Energy. *Nat. Mater.* **2017**, *16*, 16−22.
(2) Cui, X.; Liu, Y.; Chen, Y. Ultrafast Micro/Nano-Manufacturing of Metastable Materials for Energy. *Natl. Sci. Rev.* **2024**, *11* (4), nwae033.
(3) Fielden, S. D. P. Kinetically Controlled and Nonequilibrium Assembly of Block Copolymers in Solution. *J. Am. Chem. Soc.* **2024**, *146* (28), 18781−18796.
(4) Mitchell, S.; Qin, R.; Zheng, N.; Pérez-Ramírez, J. Nanoscale Engineering of Catalytic Materials for Sustainable Technologies. *Nat. Nanotechnol.* **2021**, *16* (2), 129−139.
(5) Li, Z.; Gan, M.; Wang, Y.; Liu, Y.; Han, J.; Li, S.; Guo, J.; Qian, L. Superior Activity and Durability of Co_3Mo Correlated with Interfacial Microenvironment for Hydrogen Evolution. *Appl. Catal. B Environ. Energy* **2024**, *358*, 124395.
(6) Yu, Z.; Zhu, L.; Xu, H.; Cheng, D. Selective Enhancement of Ethylene Epoxidation via Directing Reaction Pathways over Ag Single-Atom Catalyst. *Ind. Eng. Chem. Res.* **2024**, *63* (7), 3044−3056.
(7) Dai, Y.; Li, H.; Wang, C.; Xue, W.; Zhang, M.; Zhao, D.; Xue, J.; Li, J.; Luo, L.; Liu, C.; Li, X.; Cui, P.; Jiang, Q.; Zheng, T.; Gu, S.; Zhang, Y.; Xiao, J.; Xia, C.; Zeng, J. Manipulating Local Coordination of Copper Single Atom Catalyst Enables Efficient CO_2-to-CH_4 Conversion. *Nat. Commun.* **2023**, *14*, 3382.
(8) Pan, H.; Xie, D.; Li, J.; Xie, H.; Huang, Q.; Yang, Q.; Qin, G. Development of Novel Lightweight and Cost-Effective Mg-Ce-Al Wrought Alloy with High Strength. *Mater. Res. Lett.* **2021**, *9* (8), 329−335.
(9) Tan, X.; Lu, W.; Rao, X. Effect of Ultra-Fast Heating on Microstructure and Mechanical Properties of Cold-Rolled Low-Carbon Low-Alloy Q&P Steels with Different Austenitizing Temperature. *Mater. Charact.* **2022**, *191*, 112086.
(10) Zhang, W.; Xu, J. Advanced Lightweight Materials for Automobiles: A Review. *Mater. Des.* **2022**, *221*, 110994.
(11) Zhu, W.; Gao, X.; Yao, Y.; Hu, S.; Li, Z.; Teng, Y.; Wang, H.; Gong, H.; Chen, Z.; Yang, Y. Nanostructured High Entropy Alloys as Structural and Functional Materials. *ACS Nano* **2024**, *18* (20), 12672−12706.
(12) Mishra, R. S.; Gupta, S. Microstructural Engineering through High Enthalpy States: Implications for Far-From-Equilibrium Processing of Structural Alloys. *Front. Met. Alloy.* **2023**, *2*, 1135481.
(13) Sorrenti, A.; Leira-Iglesias, J.; Markvoort, A. J.; de Greef, T. F. A.; Hermans, T. M. Non-Equilibrium Supramolecular Polymerization. *Chem. Soc. Rev.* **2017**, *46* (18), 5476−5490.
(14) Yao, Y.; Dong, Q.; Brozena, A.; Luo, J.; Miao, J.; Chi, M.; Wang, C.; Kevrekidis, I. G.; Ren, Z. J.; Greeley, J.; Wang, G.; Anapolsky, A.; Hu, L. High-Entropy Nanoparticles: Synthesis-Structure-Property Relationships and Data-Driven Discovery. *Science* **2022**, *376* (6589), No. eabn3103.
(15) McDonald, M. N.; Zhu, Q.; Paxton, W. F.; Peterson, C. K.; Tree, D. R. Active Control of Equilibrium, Near-Equilibrium, and Far-From-Equilibrium Colloidal Systems. *Soft Matter* **2023**, *19* (9), 1675−1694.
(16) Jung, C.; Ihm, Y.; Cho, D. H.; Lee, H.; Nam, D.; Kim, S.; Eom, I. T.; Park, J.; Kim, C.; Kim, Y.; Fan, J.; Ji, N.; Morris, J. R.; Owada, S.; Tono, K.; Shim, J. H.; Jiang, H.; Yabashi, M.; Ishikawa, T.; Noh, D. Y.; Song, C. Inducing Thermodynamically Blocked Atomic Ordering via Strongly Driven Nonequilibrium Kinetics. *Sci. Adv.* **2021**, *7* (52), No. eabj8552.
(17) Haugerud, I. S.; Jaiswal, P.; Weber, C. A. Nonequilibrium Wet-Dry Cycling Acts as a Catalyst for Chemical Reactions. *J. Phys. Chem. B* **2024**, *128* (7), 1724−1736.
(18) Tong, X.; Zhang, Y.-E.; Shang, B.; Zhang, H.-P.; Li, Z.; Zhang, Y.; Wang, G.; Liu, Y.; Zhao, Y.; Zhang, B.; Ke, H.; Zhou, J.; Bai, H.; Wang, W. Breaking the Vitrification Limitation of Monatomic Metals. *Nat. Mater.* **2024**, *23*, 1193−1199.
(19) Thanh, N. T. K.; Maclean, N.; Mahiddine, S. Mechanisms of Nucleation and Growth of Nanoparticles in Solution. *Chem. Rev.* **2014**, *114* (15), 7610−7630.
(20) Min, Y.; Kwak, J.; Soon, A.; Jeong, U. Nonstoichiometric Nucleation and Growth of Multicomponent Nanocrystals in Solution. *Acc. Chem. Res.* **2014**, *47* (10), 2887−2893.
(21) Xue, H.; Yang, C.; De Geuser, F.; Zhang, P.; Zhang, J.; Chen, B.; Liu, F.; Peng, Y.; Bian, J.; Liu, G.; Deschamps, A.; Sun, J. Highly Stable Coherent Nanoprecipitates via Diffusion-Dominated Solute Uptake and Interstitial Ordering. *Nat. Mater.* **2023**, *22*, 434−441.
(22) Miracle, D. B.; Senkov, O. N. A Critical Review of High Entropy Alloys and Related Concepts. *Acta Mater.* **2017**, *122*, 448−511.
(23) Silvestroni, L.; Rueschhoff, L. M.; Acord, K. A.; Castro, R.; Powell, C. Synthesis of Far-From-Equilibrium Materials for Extreme Environments. *MRS Bull.* **2022**, *47* (11), 1143−1153.
(24) Schaffter, S. W.; Chen, K. L.; O'Brien, J.; Noble, M.; Murugan, A.; Schulman, R. Standardized Excitable Elements for Scalable Engineering of Far-From-Equilibrium Chemical Networks. *Nat. Chem.* **2022**, *14* (11), 1224−1232.
(25) Linker, T.; Nomura, K.; Aditya, A.; Fukshima, S.; Kalia, R. K.; Krishnamoorthy, A.; Nakano, A.; Rajak, P.; Shimmura, K.; Shimojo, F.; Vashishta, P. Exploring Far-From-Equilibrium Ultrafast Polarization Control in Ferroelectric Oxides with Excited-State Neural Network Quantum Molecular Dynamics. *Sci. Adv.* **2022**, *8* (12), No. eabk2625.
(26) Yao, Y.; Huang, Z.; Xie, P.; Lacey, S. D.; Jacob, R. J.; Xie, H.; Chen, F.; Nie, A.; Pu, T.; Rehwoldt, M.; Yu, D.; Zachariah, M. R.; Wang, C.; Shahbazian-Yassar, R.; Li, J.; Hu, L. Carbothermal Shock Synthesis of High-Entropy-Alloy Nanoparticles. *Science* **2018**, *359* (6383), 1489−1494.
(27) Yang, C.; Ko, B. H.; Hwang, S.; Liu, Z.; Yao, Y.; Luc, W.; Cui, M.; Malkani, A. S.; Li, T.; Wang, X.; Dai, J.; Xu, B.; Wang, G.; Su, D.; Jiao, F.; Hu, L. Overcoming Immiscibility toward Bimetallic Catalyst Library. *Sci. Adv.* **2020**, *6* (17), aaz6844.
(28) Maklar, J.; Windsor, Y. W.; Nicholson, C. W.; Puppin, M.; Walmsley, P.; Esposito, V.; Porer, M.; Rittmann, J.; Leuenberger, D.; Kubli, M.; Savoini, M.; Abreu, E.; Johnson, S. L.; Beaud, P.; Ingold, G.; Staub, U.; Fisher, I. R.; Ernstorfer, R.; Wolf, M.; Rettig, L. Nonequilibrium Charge-Density-Wave Order beyond the Thermal Limit. *Nat. Commun.* **2021**, *12*, 2499.
(29) Bianchini, M.; Wang, J.; Clément, R. J.; Ouyang, B.; Xiao, P.; Kitchaev, D.; Shi, T.; Zhang, Y.; Wang, Y.; Kim, H.; Zhang, M.; Bai, J.; Wang, F.; Sun, W.; Ceder, G. The Interplay between Thermodynamics and Kinetics in the Solid-State Synthesis of Layered Oxides. *Nat. Mater.* **2020**, *19* (10), 1088−1095.
(30) Dong, Q.; Lele, A. D.; Zhao, X.; Li, S.; Cheng, S.; Wang, Y.; Cui, M.; Guo, M.; Brozena, A. H.; Lin, Y.; Li, T.; Xu, L.; Qi, A.; Kevrekidis, I. G.; Mei, J.; Pan, X.; Liu, D.; Ju, Y.; Hu, L. Depolymerization of Plastics by Means of Electrified Spatiotemporal Heating. *Nature* **2023**, *616*, 488−494.
(31) Han, Y. C.; Cao, P. Y.; Tian, Z. Q. Controllable Synthesis of Solid Catalysts by High-Temperature Pulse. *Accounts Mater. Res.* **2023**, *4* (8), 648−654.
(32) Liu, L.; Zhang, Y.; Rogozhkin, S.; Klauz, A.; Li, C.; Li, J.; Zhang, Z. Enhanced Ductility via High-Density Nanoprecipitates Driven by Chemical Supersaturation in a Flash-Heated Precipitation-Strengthened High-Entropy Alloy. *Acta Mater.* **2024**, *281*, 120434.
(33) Wen, W.; Zhao, Y.; Deng, Y.; Peng, K.; Liu, Y.; Wei, F. Soft-Hard" Microstructure Evolution and Its Relevance to High Strength-Plasticity and Low Plastic Anisotropy of Al-Mg Alloys Based on Ultra-Fast Heating. *Mater. Sci. Eng., A* **2024**, *893*, 146154.
(34) Yuan, Q.; Ren, J.; Mo, J.; Zhang, Z.; Tang, E.; Xu, G.; Xue, Z. Effects of Rapid Heating on the Phase Transformation and Grain

Refinement of a Low-Carbon Mciroalloyed Steel. *J. Mater. Res. Technol.* **2023**, *23*, 3756−3771.
(35) Li, Z.; Zhang, J.; Xiao, T.; Sun, B.; He, Y.; Liu, S.; Liu, L.; Jiao, Y.; Wu, R. Regulating Microstructure and Improving Precipitation Hardening Response of Fine-Grained Mg-RE-Ag Hot-Extruded Alloy by Extreme Short-Time Heat Treatment. *Mater. Sci. Eng., A* **2024**, *892*, 146059.
(36) Hu, C.; Yue, K.; Han, J.; Liu, X.; Liu, L.; Liu, Q.; Kong, Q.; Pao, C.-W.; Hu, Z.; Suenaga, K.; Su, D.; Zhang, Q.; Wang, X.; Tan, Y.; Huang, X. Misoriented High-Entropy Iridium Ruthenium Oxide for Acidic Water Splitting. *Sci. Adv.* **2023**, *9* (37), No. eadf9144.
(37) Xu, Z.; Meng, M.; Zhou, G.; Liang, C.; An, X.; Jiang, Y.; Zhang, Y.; Zhou, Y.; Liu, L. Half-metallization Atom-Fingerprints Achieved at Ultrafast Oxygen-Evaporated Pyrochlores for Acidic Water Oxidation. *Adv. Mater.* **2024**, *36*, 2404787.
(38) Liu, J.; You, Y.; Huang, L.; Zheng, Q.; Sun, Z.; Fang, K.; Sha, L.; Liu, M.; Zhan, X.; Zhao, J.; Han, Y. C.; Zhang, Q.; Chen, Y.; Wu, S.; Zhang, L. Precisely Tunable Instantaneous Carbon Rearrangement Enables Low-Working-Potential Hard Carbon Toward Sodium-Ion Batteries with Enhanced Energy Density. *Adv. Mater.* **2024**, *36*, 2407369.
(39) Chen, Y.; Egan, G. C.; Wan, J.; Zhu, S.; Jacob, R. J.; Zhou, W.; Dai, J.; Wang, Y.; Danner, V. A.; Yao, Y.; Fu, K.; Wang, Y.; Bao, W.; Li, T.; Zachariah, M. R.; Hu, L. Ultra-Fast Self-Assembly and Stabilization of Reactive Nanoparticles in Reduced Graphene Oxide Films. *Nat. Commun.* **2016**, *7*, 12332.
(40) Xie, H.; Hong, M.; Hitz, E. M.; Wang, X.; Cui, M.; Kline, D. J.; Zachariah, M. R.; Hu, L. High-Temperature Pulse Method for Nanoparticle Redispersion. *J. Am. Chem. Soc.* **2020**, *142* (41), 17364−17371.
(41) Dou, S.; Xu, J.; Zhang, D.; Liu, W.; Zeng, C.; Zhang, J.; Liu, Z.; Wang, H.; Liu, Y.; Wang, Y.; He, Y.; Liu, W.; Gan, W.; Chen, Y.; Yuan, Q. Ultrarapid Nanomanufacturing of High-Quality Bimetallic Anode Library toward Stable Potassium-Ion Storage. *Angew. Chem. Int. Ed.* **2023**, *62* (26), No. e202303600.
(42) Cao, X. Q.; Zhou, J.; Li, S.; Qin, G. W. Ultra-Stable Metal Nano-Catalyst Synthesis Strategy: A Perspective. *Rare Met.* **2020**, *39* (2), 113−130.
(43) Han, Y. C.; Liu, M.-L.; Sun, L.; Li, X.-C.; Yao, Y.; Zhang, C.; Ding, S. Y.; Liao, H. G.; Zhang, L.; Fan, F. R.; Moskovits, M.; Tian, Z. Q. A General Strategy for Overcoming the Trade-off between Ultrasmall Size and High Loading of MOF-Derived Metal Nanoparticles by Millisecond Pyrolysis. *Nano Energy* **2022**, *97*, 107125.
(44) Ren, J.; Zhang, Y.; Zhao, D.; Chen, Y.; Guan, S.; Liu, Y.; Liu, L.; Peng, S.; Kong, F.; Poplawsky, J. D.; Gao, G.; Voisin, T.; An, K.; Wang, Y. M.; Xie, K. Y.; Zhu, T.; Chen, W. Strong yet Ductile Nanolamellar High-Entropy Alloys by Additive Manufacturing. *Nature* **2022**, *608* (7921), 62−68.
(45) Liu, Q.; Chu, S.; Zhang, X.; Wang, Y.; Zhao, H.; Zhou, B.; Wang, H.; Wu, G.; Mao, B. Laser Shock Processing of Titanium Alloys: A Critical Review on the Microstructure Evolution and Enhanced Engineering Performance. *J. Mater. Sci. Technol.* **2025**, *209*, 262−291.
(46) DePond, P. J.; Fuller, J. C.; Khairallah, S. A.; Angus, J. R.; Guss, G.; Matthews, M. J.; Martin, A. A. Laser-Metal Interaction Dynamics during Additive Manufacturing Resolved by Detection of Thermally-Induced Electron Emission. *Commun. Mater.* **2020**, *1*, 92.
(47) Kermani, M.; Dong, J.; Biesuz, M.; Linx, Y.; Deng, H.; Sglavo, V. M.; Reece, M. J.; Hu, C.; Grasso, S. Ultrafast High-Temperature Sintering (UHS) of Fine Grained α-Al_2O_3. *J. Eur. Ceram. Soc.* **2021**, *41* (13), 6626−6633.
(48) Zhu, C.; Zhao, Z.; Zhu, Q.; Wang, G.; Zuo, Y.; Li, Q.; Qin, G. Hot-Top Direct Chill Casting Assisted by a Twin-Cooling Field: Improving the Ingot Quality of a Large-Size 2024 Al Alloy. *J. Mater. Sci. Technol.* **2022**, *112*, 114−122.
(49) Kaseem, M.; Fatimah, S.; Nashrah, N.; Ko, Y. G. Recent Progress in Surface Modification of Metals Coated by Plasma Electrolytic Oxidation: Principle, Structure, and Performance. *Prog. Mater. Sci.* **2021**, *117*, 100735.
(50) Cao, X.; Zhou, J.; Wang, H.; Li, S.; Wang, W.; Qin, G. Abnormal Thermal Stability of Sub-10 Nm Au Nanoparticles and Their High Catalytic Activity. *J. Mater. Chem. A* **2019**, *7* (18), 10980−10987.
(51) Cao, X.; Zhou, J.; Zhai, Z.; Li, S.; Yuan, G.; Qin, G. Synchronous Growth of Porous MgO and Half-Embedded Nano-Ru on a Mg Plate: A Monolithic Catalyst for Fast Hydrogen Production. *ACS Sustain. Chem. Eng.* **2021**, *9*, 3616−3623.
(52) Liao, Y.; Li, Y.; Zhao, R.; Zhang, J.; Zhao, L.; Ji, L.; Zhang, Z.; Liu, X.; Qin, G.; Zhang, X. High-Entropy-Alloy Nanoparticles with 21 Ultra-Mixed Elements for Efficient Photothermal Conversion. *Natl. Sci. Rev.* **2022**, *9* (6), nwac041.
(53) Arora, N.; Sharma, N. N. Arc Discharge Synthesis of Carbon Nanotubes: Comprehensive Review. *Diam. Relat. Mater.* **2014**, *50*, 135−150.
(54) Pham, T. V.; Kim, J. G.; Jung, J. Y.; Kim, J. H.; Cho, H.; Seo, T. H.; Lee, H.; Kim, N. D.; Kim, M. J. High Areal Capacitance of N-Doped Graphene Synthesized by Arc Discharge. *Adv. Funct. Mater.* **2019**, *29* (48), 1905511.
(55) Li, Y.; Liao, Y.; Ji, L.; Hu, C.; Zhang, Z.; Zhang, Z.; Zhao, R.; Rong, H.; Qin, G.; Zhang, X. Quinary High-Entropy-Alloy@Graphite Nanocapsules with Tunable Interfacial Impedance Matching for Optimizing Microwave Absorption. *Small* **2022**, *18* (4), 2107265.
(56) Wang, Y.; Yang, H.; Zhang, Z.; Meng, X.; Cheng, T.; Qin, G.; Li, S. Far-from-Equilibrium Electrosynthesis Ramifies High-Entropy Alloy for Alkaline Hydrogen Evolution. *J. Mater. Sci. Technol.* **2023**, *166*, 234−240.
(57) Yu, Y.; Wang, D.; Hong, Y.; Zhang, T.; Liu, C.; Chen, J.; Qin, G.; Li, S. Bulk-Immiscible CuAg Alloy Nanorods Prepared by Phase Transition from Oxides for Electrochemical CO_2 Reduction. *Chem. Commun.* **2022**, *58* (79), 11163−11166.
(58) Wang, Y.; Hall, A. S. Pulsed Electrodeposition of Metastable $Pd_{31}Bi_{12}$ Nanoparticles for Oxygen Reduction Electrocatalysis. *ACS Energy Lett.* **2020**, *5* (1), 17−22.
(59) Hu, X.; Li, J.; Zhou, Z.; Wen, L. Tandem Electroreduction of CO_2 to Programmable Acetate and Syngas via Single-Nickel-Atom-Encapsulated Copper Nanocatalysts. *ACS Mater. Lett.* **2023**, *5* (1), 85−94.
(60) Liu, Y.; Xu, C.; Yang, B.; Meng, X.; Qin, G.; Li, S. Enhancing Selectivity for Semi-Hydrogenation of Ni by Periodic Isolation in the MM′X Structure. *Catal. Sci. Technol.* **2023**, *13* (18), 5345−5350.
(61) Song, Z.; Liu, Y.; Guo, Z.; Liu, Z.; Li, Z.; Zhou, J.; Liu, W.; Liu, R.; Zhang, J.; Luo, J.; Jiang, H.; Ding, J.; Hu, W.; Chen, Y. Ultrafast Synthesis of Large-Sized and Conductive $Na_3V_2(PO_4)_2F_3$ Simultaneously Approaches High Tap Density, Rate and Cycling Capability. *Adv. Funct. Mater.* **2024**, *34* (18), 2313998.
(62) Zheng, S. H.; Wang, X. T.; Gu, Z. Y.; Lü, H. Y.; Zhang, X. Y.; Cao, J. M.; Guo, J. Z.; Deng, X. T.; Wu, Z. T.; Zeng, R. H.; Wu, X. L. Direct and Rapid Regeneration of Spent $LiFePO_4$ Cathodes via a High-Temperature Shock Strategy. *J. Power Sources* **2023**, *587*, 233697.
(63) Li, Y.; Liao, Y.; Zhang, J.; Huang, E.; Ji, L.; Zhang, Z.; Zhao, R.; Zhang, Z.; Yang, B.; Zhang, Y.; Xu, B.; Qin, G.; Zhang, X. High-Entropy-Alloy Nanoparticles with Enhanced Interband Transitions for Efficient Photothermal Conversion. *Angew. Chemie Int. Ed.* **2021**, *60* (52), 27113−27118.
(64) Li, Y.; Chen, X.; Wei, Q.; Liu, W.; Zhang, Y.; Qin, G.; Shi, Z.; Zhang, X. Oxygen-Sulfur Co-Substitutional Fe@C Nanocapsules for Improving Microwave Absorption Properties. *Sci. Bull.* **2020**, *65* (8), 623−630.
(65) Sun, Y.; Dai, S. High-Entropy Materials for Catalysis: A New Frontier. *Sci. Adv.* **2021**, *7* (20), No. eabg1600.
(66) Xin, Y.; Li, S.; Qian, Y.; Zhu, W.; Yuan, H.; Jiang, P.; Guo, R.; Wang, L. High-Entropy Alloys as a Platform for Catalysis: Progress, Challenges, and Opportunities. *ACS Catal.* **2020**, *10* (19), 11280−11306.
(67) Xie, P.; Yao, Y.; Huang, Z.; Liu, Z.; Zhang, J.; Li, T.; Wang, G.; Shahbazian-Yassar, R.; Hu, L.; Wang, C. Highly Efficient Decom-

position of Ammonia Using High-Entropy Alloy Catalysts. *Nat. Commun.* **2019**, *10*, 4011.
(68) Cui, M.; Yang, C.; Li, B.; Dong, Q.; Wu, M.; Hwang, S.; Xie, H.; Wang, X.; Wang, G.; Hu, L. High-Entropy Metal Sulfide Nanoparticles Promise High-Performance Oxygen Evolution Reaction. *Adv. Energy Mater.* **2021**, *11* (3), 2002887.
(69) Yamane, I.; Sato, K.; Ando, T.; Tadokoro, T.; Yokokura, S.; Nagahama, T.; Kato, Y.; Takeguchi, T.; Shimada, T. Ultrahigh Pressure-Induced Modification of Morphology and Performance of MOF-Derived Cu@C Electrocatalysts. *Nanoscale Adv.* **2023**, *5* (2), 493−502.

https://doi.org/10.1021/acsmaterialslett.4c01952
ACS Materials Lett. 2025, 7, 319−332